

Contents lists available at ScienceDirect

Water Research

journal homepage: www.elsevier.com/locate/watres





Evaluation of plasmon-enhanced catalytic ozonation for the abatement of micropollutants in environmental matrices

Wenwen Yang ¹, Tingting Wu ^{*}

Department of Civil and Environmental Engineering, University of Alabama in Huntsville, Huntsville, Al, 35899, United States of America

ARTICLE INFO

Keywords:
Plasmon-enhanced catalytic ozonation
Environmental matrices
Micropollutant
Kinetic model
Byproduct
Energy consumption

ABSTRACT

Advanced oxidation processes (AOPs) have been widely investigated for the treatment of recalcitrant organic pollutants. Here we report the first study on the performance evaluation in different environmental matrices of a newly-developed AOP, plasmon-enhanced catalytic ozonation with silver doped spinel ferrite (0.5wt%Ag/ MnFe₂O₄) as the catalyst, for the degradation of representative micropollutants (e.g. atrazine and atenolol). The real matrices include surface water (SW, pH 6.82), secondary effluent (SE, pH 7.22), and reverse osmosis/RO concentrate (ROC, pH 7.90) generated during water reuse. A kinetic model combining the R_{ct} concept (the ratio of the total •OH-exposure to the total O3-exposure) and expressions of transient steady state hydroxyl radical (•OH) concentrations has been successfully developed to predict the treatment performance, where the effects of major influencing factors (e.g. solution chemistry such as pH and water constituents, and operating conditions) were explicitly quantified. Bulk organic contents, carbonate/bicarbonate, and phosphate were found to be the major chemical species that influenced the target compound removal, through interactions with reactive species (e.g. •OH) and/or the solid catalysts. Lower bromate formation was observed in the plasmon-enhanced catalytic ozonation process, compared with ozonation and catalytic ozonation processes. Low energy consumption (electrical energy per order/E_{FO} 0.011-0.086 kWh/m³ for different matrices) together with low byproduct formation has demonstrated that plasmon-enhanced catalytic ozonation is a novel promising AOP for various water treatment and reuse applications.

1. Introduction

Advanced oxidation processes (AOPs) have been intensively investigated for the removal of synthetic organic compounds (e.g. micropollutants/MPs). AOPs usually involve in-situ generation of strong oxidants (e.g. hydroxyl radicals/•OH and sulfate radicals/·SO₄⁻) at sufficient amounts to achieve organics oxidation or even mineralization (Buxton et al., 1988; Glaze et al., 1987). While contaminants can be permanently destroyed instead of being merely transferred to a brine or other phases for further treatment/disposal, AOPs are usually energy intensive and may generate undesired byproducts (Bergmann et al., 2014; Fatta-Kassinos et al., 2011; Hodges et al., 2018). In an effort to address these challenges, our research group have developed a novel heterogeneous catalytic ozonation process, utilizing the localized surface plasmon resonance (LSPR) of plasmonic nanoparticles doped on the spinel ferrite substrate (e.g. Ag/MnFe₂O₄) to achieve accelerated ozone decomposition and subsequent generation of reactive species for the

degradation of recalcitrant pollutants. And ~35 fold and ~7 fold increases in the degradation rates were achieved with a very low photon input ($\sim 10^{-10}$ Einstein L⁻¹• s⁻¹) at the plasmon band of Ag (~ 470 nm), as compared to ozonation alone and catalytic ozonation (i.e. with catalysts but without light irradiation) respectively (Yang et al., 2021). The high efficiency of pollutant abatement was also demonstrated in tap water under realistic water treatment conditions with low bromate formation (< 7 µg/L) (Yang et al., 2021). In spite of the promising performance of plasmon-enhanced catalytic ozonation, further evaluation in environmental matrices particularly the more challenging ones (e.g. secondary effluent and reverse osmosis/RO concentrate) is needed, as the solution chemistry is known to have profound effects on the treatment efficiency (Jiang et al., 2013; Kasprzyk-Hordern et al., 2003; Petrie et al., 2014). Investigation and interpretation of such effects, preferably in a quantitative approach, can not only deepen our understanding of this novel treatment process, but also provide useful information and guidelines for practical applications.

E-mail address: Tingting.Wu@uah.edu (T. Wu).

^{*} Corresponding author.

Present address: School of Environment and Safety Engineering, Jiangsu University, Zhenjiang, Jiangsu Province, 212013, China

Ozone has long been used in water treatment. In order to provide quantitative information of the major oxidants in ozonation systems, the R_{ct} concept (Eq. 1) was introduced to represent the ratio of the total \bullet OH-exposure to the total O₃-exposure (Elovitz and Von Gunten, 1999).

$$R_{ct} = \frac{\int [\bullet OH]dt}{\int [O_3]dt}$$
 (Eq. 1)

Both O_3 and $\bullet OH$ can contribute to the degradation of the target micropollutant (MP) as shown in Eqs. 2 & 3:

$$-\frac{d[MP]}{dt} = k_{O3/MP}[O_3][MP] + k_{OH/MP}[\bullet OH][MP]$$
 (Eq. 2)

$$ln\left(\frac{[MP]_0}{[MP]_t}\right) = k_{O3/MP} \int [O_3]dt + k_{\cdot OH/MP} \int [\bullet OH]dt$$

$$= \left(k_{O3/MP} + k_{\cdot OH/MP}R_{ct}\right) \int [O_3]dt$$
 (Eq. 3)

Furthermore, environmental matrices are complicated and different species may play various roles such as initiators, promoters, and inhibitors in the generation, propagation, inhibition, and/or termination of •OH. For example, some inorganic species (e.g. $HCO_3^-/CO_3^2^-$ and $PO_4^3^-$) can inhibit degradation of the target compounds by acting as radical scavengers and/or competing for the reactive sites on catalysts (Staehelin and Hoigne, 1985; Wang et al., 2018a; Yong and Lin, 2012). Moreover, the bulk organics in different environmental waters (e.g. natural organic matters/NOM and effluent organic matters/EfOM), which usually exist in much higher concentrations than that of the target pollutant, can also competitively consume ozone and/or the reactive species generated upon ozone decomposition, thus negatively influencing the treatment performance (Jiang et al., 2013; Petrie et al., 2014; Rivera-Utrilla et al., 2013). To this end, an expression of the transient steady-state •OH concentration has been developed (Staehelin and Hoigne, 1985):

$$[\bullet OH]_{ss} = \frac{2k_1[OH^-] + \sum_{s,i} [M_{l,i}]}{\sum_{s,i} [M_{s,i}]} [O_3]$$
 (Eq. 4)

where k_1 represents the rate constant of OH^- with O_3 , $k_{I,i}$ and $k_{s,i}$ represent the rate constants of initiator $(M_{I,i})$ and inhibitor $(M_{s,i})$ with $\bullet OH$, respectively, and $[M_{I,i}]$ and $[M_{s,i}]$ represent the concentrations of initiators and inhibitors, respectively. Hence, by combining the R_{ct} concept and the expression of transient steady state $\bullet OH$ concentration, it is possible to investigate and evaluate the respective effects of different influencing factors (e.g. chemical species or operating conditions) that are applicable to the specific system of interest on the degradation of the target pollutant (Yong and Lin, 2012).

The main objective of this study was to evaluate the performance of plasmon-enhanced catalytic ozonation for the abatement of representative micropollutants in different environmental matrices, i.e. surface water (SW), secondary effluent (SE), and RO concentrate (ROC) generated during water reuse. Ag/MnFe₂O₄ with stable mineralogical structures and great plasmon-responsive catalytic reactivity was used as the catalyst and monochromatic light-emitting diode (LED) at the Ag plasmon band (470 nm) was employed as the light source. Atrazine (ATZ) and atenolol (ATL), both of environmental significance (Esplugas et al., 2007; Petrie et al., 2014) and with low to medium reactivity with ozone ($k_{O3/ATZ} = 6.0 \text{ M}^{-1} \bullet \text{s}^{-1}, k_{\bullet OH/ATZ} = 3 \times 10^9 \text{ M}^{-1} \bullet \text{s}^{-1} \text{(Acero et al., 2000)}, k_{O3/ATL} = 1.7 \times 10^3 \text{ M}^{-1} \bullet \text{s}^{-1}, k_{\bullet OH/ATL} = 8 \times 10^9 \text{ M}^{-1} \bullet \text{s}^{-1}$ (Márquez et al., 2014; Wu et al., 2019)), were selected as the model compounds. Here, we first examined ATZ removal during plasmon-enhanced catalytic ozonation in different matrices and further identified the major chemical species that influenced the overall performance. In the following study, we quantitatively evaluated these effects and developed a semi-empirical kinetic model utilizing the R_{ct} concept and expressions of [•OH]ss, which explicitly incorporated the major influencing operating and water chemistry parameters. The

validity of the model was then examined by comparing the time-dependent degradation of ATL predicted by the model with that measured experimentally under different operating and solution chemical conditions. Bromate formation was also monitored during the runs. Lastly, the electrical energy per order ($E_{\rm EO}$) was estimated for the treatment of different environmental matrices. Research results of this study can provide first-hand quantitative information on the applicability and guidelines of plasmon-enhanced catalytic ozonation for practical applications.

2. Materials and methods

2.1. Chemicals and reagents

Iron nitrate nonahydrate (Fe(NO₃)₃ • 9H₂O, Acros Organic), silver nitrate (AgNO₃, Alfa Aesar), and manganese nitrate tetrahydrate (Mn (NO₃)₂ • 4H₂O, Acros Organic) were the metal sources for the catalyst preparation, where citric acid (Fisher Scientific) was used as the fuel for auto-combustion and ammonium hydroxide (28%-35% w/w, Fisher Scientific) was used to adjust pH. Atrazine (CAS#: 1912–24–9) and atenolol (ATL, CAS#: 29,122–68–7) were obtained from Sigma-Aldrich. t - Butanol (TBA) (Fisher Scientific) was added as an external inhibitor. All chemicals were of analytical grade and used without further purification.

2.2. Samples of environmental matrices

Environmental matrices tested in this study include surface water (SW; after coagulation and sand filtration but before disinfection), secondary effluent (SE; filtered through 0.45 μm membrane filter), and reverse osmosis concentrate (ROC) generated from wastewater reuse. Samples of SW and SE were collected from local treatment plants. ROC was generated using a lab-scale RO skid (RO membrane: FILMTEC^TM TW30–1812–36) with SE as the feed water. The recovery rate was controlled at $\sim\!\!75\%$. All samples of environmental matrices were stored at 4 °C until use. The main matrix characteristics are summarized in Table S1. It is noted that the SE sample collected in this study was of low strength, i.e. low organic content.

2.3. Catalyst synthesis and ozonation experiments

Catalysts (0.5wt%Ag/MnFe₂O₄) were synthesized via a facile one-pot auto-combustion method followed by H_2 reduction as detailed in our previous study (Yang et al., 2021) and in the supporting information (SI, Text S1).

Plasmon-enhanced catalytic ozonation experiments were conducted in a semi-batch reactor where ozone feed gas was continuously bubbled into a 250 mL cylindrical quartz reactor (Yang and Wu, 2019). Pure oxygen (O₂) was used as the feeding gas for ozone (O₃) generation by an ozone generator (MP5000, A2Z Ozone Inc, USA). Ozone gas was injected at the bottom of reactor with a diffuser stone (quartzes porous plate) at a flow rate of 0.1 L/min at working temperature and pressure. The concentration of feeding O₃ as well as that in the offgas line was continuously monitored using two ozone analyzers (API-454). Hence the transferred ozone dose (TOD, mg/L) during the experiment can be calculated from Eq. 5:

$$TOD = \int_{0}^{r} \frac{Q_{gas}}{V} \cdot ([O_3]_{inlet} - [O_3]_{outlet}) \cdot dt$$
 (Eq. 5)

where $[O_3]_{inlet}$ and $[O_3]_{outlet}$ are ozone concentrations in the feeding line and off gas line respectively, mg/L; Q_{gas} is gas flow into the reactor, 0.1 L/min; V is the volume of the working solution, L; t is the treatment time, min

For a typical run, 0.20 g solid catalysts were added into 150 mL

working solution spiked with the desired amount of model compounds. Two LED lights ($\lambda=470$ nm) were used as the light source and photon flux dosed into the reactor during the run was determined using chemical actinometry (Yang et al., 2021). pH was monitored but not adjusted during the run. Samples were taken at pre-determined time intervals and quenched by $\rm Na_2S_2O_3$ to dissipate the residual ozone, and then filtered through an ozone-resistant filter (Millipore PVDF, 0.45 μm) to separate the catalyst. Preliminary tests confirmed that $\rm Na_2S_2O_3$ quenching and filtration did not affect analytical measurement of the target compounds. Control experiments of catalytic ozonation and ozonation were conducted under the same conditions without catalysts and/or light irradiation. All experiments were conducted at least in duplicates and the error bars in the figures represent the standard deviations.

2.4. Analytical methods

Low concentrations of atrazine (ATZ) and atenolol (ATL) (< 0.03 mg/L) were measured using HPLC/MS/MS (DionEX UltiMate 3000-LTQ Orbitrap XL) in positive electrospray ionization (ESI) mode (Text S2). Higher concentrations of atrazine and atenolol were determined using high performance liquid chromatography (HPLC/DAD, Agilent 1100 series) with a reversed-phase luna C-18 analytic column (Aglient 1100) at $\lambda = 230$ nm and $\lambda = 224$ nm, respectively (Text S2). Total organic carbon (TOC) was measured with a Shimadzu TOC-LCPH analyzer. PO_4^{3-} was measured using Hach method 8048 (0.02 – 2.50 mg/L). Alkalinity was determined according to the standard Method 2320 B (Clesceri et al., 2009). Concentrations of Cl⁻, NO₃⁻, SO₄²⁻, Br⁻, and BrO₃ were determined using an ion chromatography (Dionex ICS-1600, USA) equipped with an AG19 pre-guard and AS19 separating column, and potassium oxide (KOH) solution (18 mM) and DI water were used as the mobile phase with a flow rate of 1.0 mL/min and injection volume 25 µL. HOBr/OBr- was determined after quenching the reaction by adding 0.5 mM phenol at pH 3. These species are stable and were analyzed by HPLC/UV (column: RP luna C-18; eluent: 50% of a 0.2% acetic acid and 50% methanol, 1 mL/min; sample volume: 20 µL; UV-detection at 225 nm) (Pinkernell and Von Gunten, 2001). The concentration of dissolved ozone (DO₃) was determined with the indigo method Bader (1982).

3. Results and discussion

3.1. Catalyst characteristics

The catalysts (0.5wt%Ag/MnFe₂O₄) used in this study have been fully characterized by X-Ray diffraction (XRD), high resolution transmission electron microscopy (HR-TEM), X-ray absorption spectroscopy (XAS) measurements including X-ray absorption near edge structure (XANES) and extended X-ray absorption fine structure (EXAFS), and Xray photoelectron spectroscopy (XPS) in our previous study (Yang et al., 2021). Briefly, XRD patterns of the catalyst matched the standard JCPDS (card no. 10-0319) for the magnetic MnFe₂O₄ spinel and Ag doping did not change the spinel structure. Linear combination fitting (LCF) of Ag K-edge XANES spectra indicated Ag⁰ and Ag⁺ accounted for 22% and 78% of Ag in the bulk catalyst respectively. A general formula [Mn_{0.22} $Fe_{0.78}$] A $[Mn_{0.78}Fe_{1.22}]$ BO₄ was derived based on extended X-ray absorption fine structure (EXAFS) fitting, where A and B represent the tetrahedral and octahedral sites respectively. XPS analyses showed Ag (0 and +1), Fe (+2 and +3), and Mn (+2 and +3) were present on the catalyst surface. In this study, Fourier Transformed Infrared (ATR-FTIR) spectra were also employed to study the surface acidic properties of catalysts with different Ag doping using pyridine as a probe molecular (Figure S1; Text S3). The results showed that 0.5wt% Ag/MnFe₂O₄ catalyst may have more Lewis acidic sites than 0.25wt% Ag/MnFe₂O₄ and 1wt% Ag/MnFe₂O₄, which agrees well with our previous study (Yang et al., 2021). The scanning transmission electron microscopy

(STEM) images of the catalysts are shown in Figure S2.

3.2. Performance of plasmon-enhanced catalytic ozonation in environmental matrices

Performance of plasmon-enhanced catalytic ozonation for the removal of the model compound ATZ was first examined in different environmental matrices, including surface water (SW), secondary effluent (SE), and RO concentrate (ROC) produced as described in Section 2.2. Experiments of ozonation alone and catalytic ozonation (i.e. without light irradiation) were also conducted under otherwise same conditions for comparison. As shown in Fig. 1(A-C), in all three matrices ATZ degradation generally followed a global first order kinetics, where the fastest removal was achieved in plasmon-enhanced catalytic ozonation, followed by catalytic ozonation and then ozonation, at the same transferred ozone dose (Eq. 5). These results confirmed the superior performance of plasmon-enhanced catalytic ozonation even in DOMrich environmental matrices. Moreover, although the mass ratio of transferred ozone to DOC was kept constant (i.e. 0.85) in different matrices, the rate of ATZ degradation followed the order $k_{\text{ATZ}} = 0.397$ min^{-1} (SW) $> k_{ATZ} = 0.189 \ min^{-1}$ (SE) $> k_{ATZ} = 0.116 \ min^{-1}$ (ROC) in plasmon-enhanced catalytic ozonation processes, clearly demonstrating the matrix effects (Fig. 1D).

Since ATZ has a very low reactivity with O₃, its degradation during plasmon-enhanced catalytic ozonation was mainly contributed to the reactive species generated upon ozone decomposition (e.g. •OH, O₂•-, and ¹O₂) (Yang et al., 2021). It is well known that presence of various organic and inorganic species can influence ozone decomposition in water, which may act as either initiators (e.g. -OH) reacting directly with O_3 for the generation of $O_2^- \bullet$ or $\bullet O_3^-$ and subsequent $\bullet OH$ formation, or inhibitors terminating the chain reactions after reacting with •OH (e.g. HCO₃⁻/CO₃²⁻ and PO₄³⁻) (Staehelin and Hoigne, 1985; Yong and Lin, 2012). Furthermore, usually dissociative adsorption of ozone on the active sites is an important step during heterogeneous catalytic ozonation for the generation of various reactive species. For example, we think the accelerated ozone decomposition during plasmon-enhanced catalytic ozonation with Ag/MnFe₂O₄ as the catalysts was achieved through energy transferred from plasmonic Ag nanostructures to ozone adsorptive sites (e.g. surface -OH groups) during LSPR decay at both existing and newly-activated catalytic active sites (Yang et al., 2021). Hence, interactions between different species present in the water matrices and the catalyst active sites can also affect, likely negatively, ozone decomposition through the dissociative adsorption pathway. Environmental waters are complicated matrices where both bulk organics (e.g. natural organic matters/NOM in SW and effluent organic matters/EfOM in SE) and various inorganic species along with the target pollutants co-exist. These substances may initiate or inhibit ozone decomposition, scavenge the radical species, or occupy/block surface active sites for ozone adsorption. For example, phosphate has often been employed as a strong Lewis base to probe the role of surface -OH groups as active sites for ozone decomposition in heterogeneous catalytic ozonation (Sun et al., 2014; ;(Wang et al., 2018b) Zhao et al., 2013).

In an effort to elucidate the effects of specific chemical species commonly present in environmental waters on the abatement of target pollutants in plasmon-enhanced catalytic ozonation processes, we first evaluated the removal of ATZ in deionized (DI) water as well as synthetic matrices, which simulated the major inorganic contents in the environmental samples but without organic matters (S-SW, S-SE, and S-ROC, Table S1). As shown in Fig. 2, while > 95% was degraded in the DI matrix in 5 min, ATZ removal was lower in synthetic solutions, i.e. 90% in synthetic SW, 73% in synthetic SE, and 58% in synthetic ROC, confirming the influence of inorganic species. On the other hand, better performance in these synthetic solutions than that in the corresponding real environmental matrices also demonstrated the effects of organic matters. Further, upon a closer look, it can be seen that difference between the synthetic and real water samples was less pronounced than

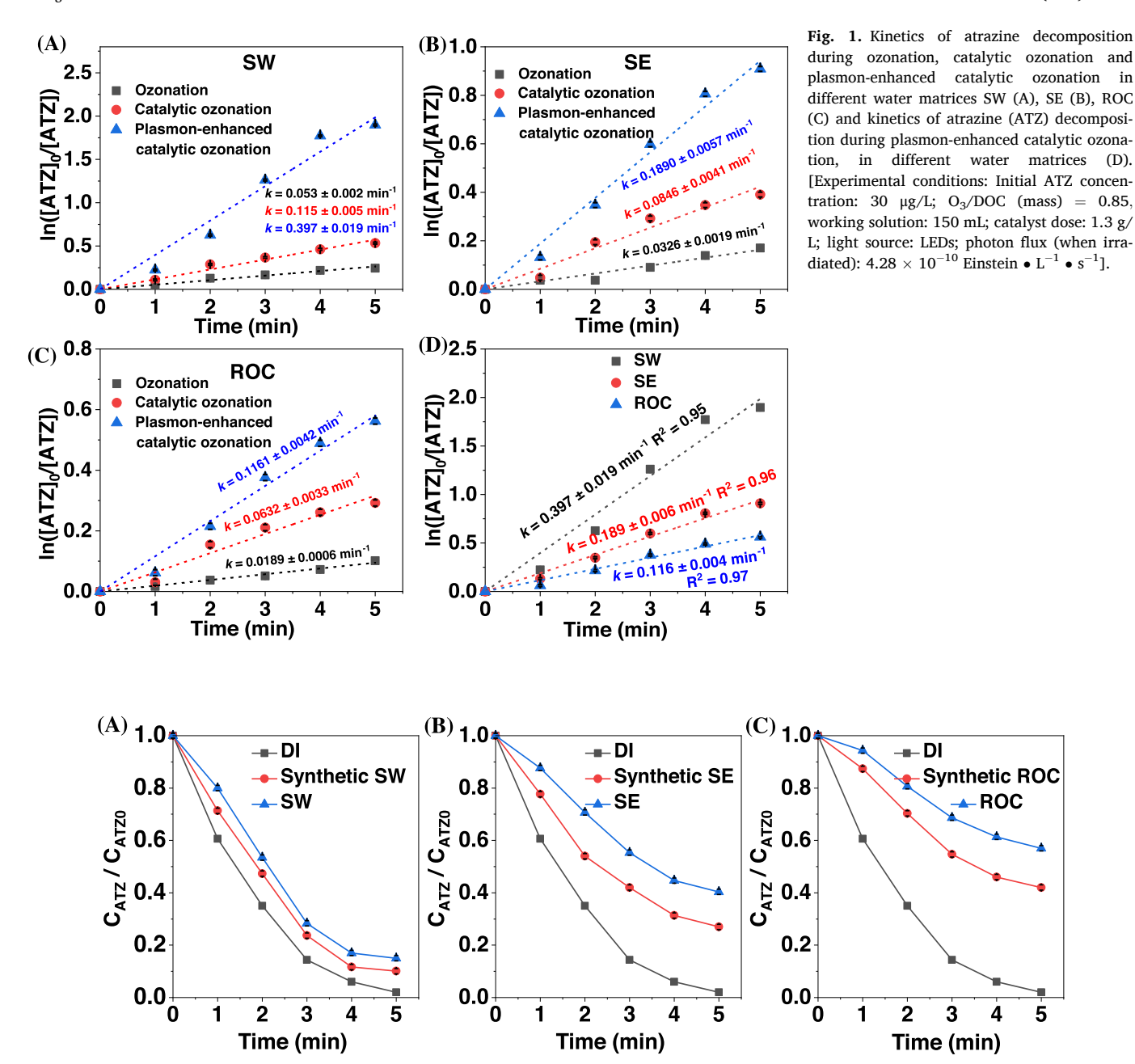


Fig. 2. Influence of inorganic anions and bulk organic matters on ATZ removal [Experimental conditions: Initial ATZ concentration: 30 μ g/L; feed gas O_3 concentration: (A) 2.56 mg/L, (B) 3.61 mg/L, (C) 8.96 mg/L; working solution: 150 mL; catalyst dose: 1.3 g/L; light source: LEDs; photon flux: 4.28×10^{-10} Einstein • L^{-1} • s^{-1}].

that between DI and synthetic solutions especially for SE and ROC, indicating the important role of inorganic species particularly at relatively high concentrations. To further identify the main inorganic species that inhibit the degradation of the target pollutant, we examined ATZ degradation during plasmon-enhanced catalytic ozonation in the presence of several common inorganic anions, including phosphate, carbonate/bicarbonate (alkalinity), sulfate, chloride, and nitrate, within the typical concentration range in environmental waters. As shown in Fig. 3, while choride, sulfate, and nitrate had minimum effects, phosphate and carbonate/biocarbonate clearly inhibited ATZ removal, likely due to scavenging of reactive species and/or competitive occupancy of the ozone adsorption sites on the catalysts.

3.3. Development of kinetic models for the degradation of target pollutants in plasmon-enhanced catalytic ozonation processes utilizing the R_{ct} concept and $[\cdot OH]_{ss}$

Results and discussion of Section 3.2 have laid a good groundwork for developing kinetic models for the removal of target pollutants in environmental matrices based on Eqs 1–4. This approach was selected because the effects of major influencing factors (e.g. solution chemistry and operating parameters) are explicitly expressed in a quantitative way, which may be particularly appealing for practical applications because prediction of the treatment performance under different conditions becomes possible. In plasmon-enhanced catalytic ozonation processes, hydroxyl ions/OH⁻, NOM/EfOM, and catalyst & light irradiation contribute to the total initiation capacity, while the total inhibition capacity can be taken as the additive effects of NOM/EfOM,

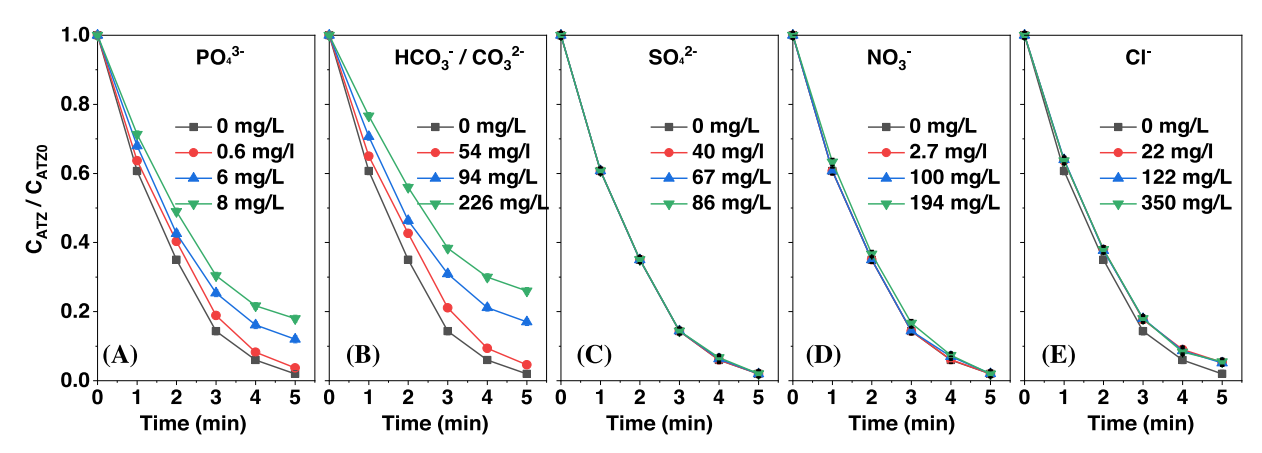


Fig. 3. Influence of inorganic anions PO_4^{3-} (A), Initial HCO_3^{-}/CO_3^{2-} (as mg/L CaCO₃) (B), SO_4^{2-} (C), NO_3^{-} (D), and Cl (E) on ATZ removal [Experimental conditions: Initial ATZ concentration: 30 μ g/L; O_3/TOC (mass) = 2.5; working solution: 150 mL; catalyst dose: 1.3 g/L; light source: LEDs; photon flux: 4.28×10^{-10} Einstein \bullet L⁻¹ \bullet s⁻¹; $pH_0 = 7.0$].

 ${\rm HCO_3}^-/{\rm CO_3}^{2-}$, and ${\rm PO_4}^{3-}$. It should be noted that NOM/EfOM can simultaneously act as the initiator, promoter, and inhibitor in ozonation processes (Staehelin and Hoigne, 1985). Although they do not affect the R_{ct} value, promoters can propagate the radical chain reactions (Yong and Lin, 2012). Moreover, we have confirmed the validity of surface $-{\rm OH}$ density to represent the ozone adsorption capacity in our previous study with the same experimental setup, and have demonstrated the rate constants of ozone decomposition as well as those of the model compound degradation changed proportionally to the photon flux in the plasmon-enhanced catalytic ozonation process (Yang et al., 2021). Therefore, Eq. 4 can be rewritten as the following equation:

$$[\bullet \text{OH}]_{ss} = \frac{2k_{1}[OH^{-}] + \left((k_{2}) \times \left(\frac{[O_{3}]_{(adsmax)}K_{I1}}{1 + K_{I1}[O_{3}]_{a}}\right) \times (\rho \times [catalyst])\right) + k_{I2}[TOC]}{k_{s2}[TOC] + k_{3}\left[HCO_{3}^{-}\right] + k_{4}\left[PO_{4}^{3-}\right]} [O_{3}]$$
(Eq. 6)

where k_1 represents the rate constant of -OH with O_3 , $M^{-1} \bullet s^{-1}$; k_2 is the rate constant of catalyst, $M^{-1} \bullet s^{-1}$; K_{II} is the constant of adsorption equilibrium of Langmuir-Hinshelwood (L-H), M⁻¹; [O₃]_a is the steadystate dissolved ozone concentration, M; [O₃]_{ads max} is the maximum coverage concentration of the adsorbed ozone, M; ρ is the density of surface -OH groups, mol/g; [catalyst] is the catalyst dose, g/L; k_{12} and k_{s2} represent the initiation and the inhibition rate constants of NOM /EfOM, respectively, $M^{-1} \bullet s^{-1}$: [TOC] represent the concentrations of NOM/ EfOM as total organic carbon/C, M; k_3 and k_4 represent the inhibition rate constants of HCO_3^-/CO_3^{2-} and PO_4^{3-} , respectively, $M^{-1} \bullet s^{-1}$; and [HCO_3^-] and [PO_4^{3-}] represent the concentrations of HCO_3^-/CO_3^{2-} and PO₄³⁻, respectively, M. Furthermore, as shown in Text S4 (a), the coefficient of [O₃] in Eq. 4 equals to the numerical value of R_{ct}. Since R_{ct} can be experimentally determined by monitoring the degradation of a model compound using Eq. 3, the values of the different initiation and inhibition rate constants in the coefficient can also be determined. In the following sections, different sets of experiments were conducted to determine values of k_1 , k_2 , K_{I1} , k_{I2} , k_{S2} , k_3 , and k_4 with ATZ as the model pollutant.

3.3.1. Determination of initiation rate constants of OH $^-$ (k_1) and Ag doped MnFe₂O₄ catalysts (k_2)

The reaction rate constant of OH $^-$ with O $_3$, k_1 , has been reported to be 70 M $^{-1} \bullet s^{-1}$ and 160 M $^{-1} \bullet s^{-1}$ (Staehelin and Holgné, 1982; Yong and Lin, 2012), with the former being determined in the presence of 10 mM HCO $_3$ $^-$ (CO $_3$ 2 $^-$ and 50 mM PO $_4$ 3 $^-$ (Staehelin and Holgné, 1982). In this study we try to delineate each initiator/inhibitor separately, hence ozonation of ATZ in DI matrices were first carried out in a semi-batch reactor at different initial pH within the relative narrow range of

environmental waters (6.8–8), where tert-butanol (TBA; $k_{\bullet OH/TBA}$ =5.0 \times 10^8 M^{-1} \bullet s^{-1}) was added as an external inhibitor. Under these conditions, Eq. 6 can be simplified as:

$$[\bullet OH]_{ss} = \frac{2k_1[OH^-]}{k_{\bullet OH/TBA}[TBA]}[O_3]$$
 (Eq. 7)

As expected, higher pH led to faster ATZ degradation (Figure S3A). Moreover, as can be seen in Figure S3B, pH remained relatively constant during the runs. Therefore, [OH $^-$] may be approximated using the initial pH. R_{ct} values at different pH can be computed based on experimental data of ATZ degradation using Eq. 3 (Figure S4A). k_1 can then be determined from the slope of the plot of R_{ct} vs [OH $^-$], which is found to be 144.6 $M^{-1} \bullet s^{-1}$ here (Figure S4B). This value is close to the reported value of 160 $M^{-1} \bullet s^{-1}$ and is used in the following studies.

It is worth emphasizing that plasmon-enhanced catalytic ozonation is a highly complex system involving three phases as well as light irradiation. While our previous research effort was devoted to understand the underlying mechanisms of plasmon-induced enhancement, the objectives of this study were to evaluate the process performance in real environmental matrices, and further to develop a semi-empirical model with major operating parameters and influencing chemical species as the input for convenient practical applications. Therefore, in order to quantitatively evaluate the contribution of catalysts/light irradiation to ozone decomposition, a mass balance approach was employed. Several sets of semi-batch ozone decomposition experiments were conducted in the presence of catalysts with light irradiation in DI matrices (to eliminate effects of other chemical species). The initial pH was set at 7.00 and the variation was within \pm 0.20 during the runs. Under these conditions, a mass balance analysis of ozone at steady-state yields:

$$Q_{gas}([O_3]_{inlet} - [O_3]_{outlet}) = r \times V$$
 (Eq. 8)

where r is the overall ozone decomposition rate and other parameters are defined in Eq (5).

Here ozone may be decomposed via both homogeneous pathways $(r_1 = k_1[\text{-OH}] \times [O_3]_a)$ and heterogeneous pathways $(r_2 = k_2\text{'}[\text{-OH}]_{\text{surface}} \times [O_3]_a = (k_2 \times \frac{[O_3]_{\text{ols.-max}} K_1}{1+K_1[O_3]_a}) \times [\text{-OH}]_{\text{surface}} \times [O_3]_a$, Text S4). However, under the experimental conditions here, homogeneous ozone decomposition may be neglected as the rate was very low $(r_1 < 10^{-5} \text{ M} \cdot \text{s}^{-1}, r \sim 3.6 \times 10^{-3} \text{ M} \cdot \text{s}^{-1})$. Hence, Eq (8) can be rewritten as:

$$\begin{split} \left(Q_{gas}\left(\left[O_{3}\right]_{inlet}-\left[O_{3}\right]_{outlet}\right)\right)\bigg/V &= \left(k_{2} \times \frac{\left[O_{3}\right]_{(ads_max)}K_{I1}}{1+K_{I1}\left[O_{3}\right]_{a}}\right) \times \left[-\text{OH}\right]_{surface} \\ &\times \left[O_{3}\right]_{a} \end{split} \tag{Eq. 9}$$

By varying the feed gas concentration, a linear relationship of $1/r_2$ vs $1/[O_3]_a$ was obtained and the rate constant (k_2) and the constant of adsorption equilibrium constant of L–H (K_{II}) under certain photon flux were determined from the slope and the intercept of the plots (Figure S5A; Eqs S7;Text S4(b)). To further investigate the effects of photon inputs on k_2 , plots of $1/r_2$ vs $1/[O_3]_a$ were also obtained at different photon flux $(3.1 \times 10^{-10} \ \mathrm{Einstein} \bullet \ \mathrm{L}^{-1} \bullet \ \mathrm{s}^{-1} \sim 6.4 \times 10^{-10} \ \mathrm{Einstein} \bullet \ \mathrm{L}^{-1} \bullet \ \mathrm{s}^{-1} \sim 6.4 \times 10^{-10} \ \mathrm{Einstein} \bullet \ \mathrm{L}^{-1} \bullet \ \mathrm{s}^{-1} \sim 6.4 \times 10^{-10} \ \mathrm{Einstein} \bullet \ \mathrm{L}^{-1} \bullet \ \mathrm{s}^{-1} \sim 6.4 \times 10^{-10} \ \mathrm{Einstein} \bullet \ \mathrm{L}^{-1} \bullet \ \mathrm{S}^{-1} \sim 6.4 \times 10^{-10} \ \mathrm{Einstein} \bullet \ \mathrm{L}^{-1} \bullet \ \mathrm{S}^{-1} \sim 6.4 \times 10^{-10} \ \mathrm{Einstein} \bullet \ \mathrm{L}^{-1} \bullet \ \mathrm{S}^{-1} \sim 6.4 \times 10^{-10} \ \mathrm{Einstein} \bullet \ \mathrm{L}^{-1} \bullet \ \mathrm{S}^{-1} \sim 6.4 \times 10^{-10} \ \mathrm{Einstein} \bullet \ \mathrm{L}^{-1} \bullet \ \mathrm{S}^{-1} \sim 6.4 \times 10^{-10} \ \mathrm{Einstein} \bullet \ \mathrm{L}^{-1} \bullet \ \mathrm{S}^{-1} \sim 6.4 \times 10^{-10} \ \mathrm{Einstein} \bullet \ \mathrm{L}^{-1} \bullet \ \mathrm{S}^{-1} \sim 6.4 \times 10^{-10} \ \mathrm{Einstein} \bullet \ \mathrm{L}^{-1} \bullet \ \mathrm{S}^{-1} \sim 6.4 \times 10^{-10} \ \mathrm{Einstein} \bullet \ \mathrm{L}^{-1} \bullet \ \mathrm{S}^{-1} \sim 6.4 \times 10^{-10} \ \mathrm{Einstein} \bullet \ \mathrm{L}^{-1} \bullet \ \mathrm{S}^{-1} \sim 6.4 \times 10^{-10} \ \mathrm{Einstein} \bullet \ \mathrm{L}^{-1} \bullet \ \mathrm{S}^{-1} \sim 6.4 \times 10^{-10} \ \mathrm{Einstein} \bullet \ \mathrm{L}^{-1} \bullet \ \mathrm{S}^{-1} \sim 6.4 \times 10^{-10} \ \mathrm{Einstein} \bullet \ \mathrm{L}^{-1} \bullet \ \mathrm{S}^{-1} \sim 6.4 \times 10^{-10} \ \mathrm{Einstein} \bullet \ \mathrm{L}^{-1} \bullet \ \mathrm{S}^{-1} \sim 6.4 \times 10^{-10} \ \mathrm{Einstein} \bullet \ \mathrm{L}^{-1} \bullet \ \mathrm{S}^{-1} \sim 6.4 \times 10^{-10} \ \mathrm{Einstein} \bullet \ \mathrm{L}^{-1} \bullet \ \mathrm{S}^{-1} \sim 6.4 \times 10^{-10} \ \mathrm{Einstein} \bullet \ \mathrm{L}^{-1} \bullet \ \mathrm{S}^{-1} \sim 6.4 \times 10^{-10} \ \mathrm{Einstein} \bullet \ \mathrm{L}^{-1} \bullet \ \mathrm{S}^{-1} \sim 6.4 \times 10^{-10} \ \mathrm{Einstein} \bullet \ \mathrm{L}^{-1} \bullet \ \mathrm{S}^{-1} \sim 6.4 \times 10^{-10} \ \mathrm{Einstein} \bullet \ \mathrm{L}^{-1} \bullet \ \mathrm{Einstein} \bullet \ \mathrm{L}^{-1} \bullet \ \mathrm{Einstein} \bullet \ \mathrm{Eins$

3.3.2. Determination of inhibition rate constants of carbonate/bicarbonate (k_3) and phosphate (k_4)

To quantify the inhibition effects of HCO_3^-/CO_3^{2-} and PO_4^{3-} , experiments of ATZ degradation during plasmon-enhanced catalytic ozonation processes were carried out in the presence of HCO_3^-/CO_3^{2-} or PO_4^{3-} at different concentrations with the addition of tert-butanol as an external inhibitor. Thus, Eq. 6 becomes:

$$[\bullet OH]_{ss} = \left(\frac{2k_1[OH^-] + \left((k_2) \times \left(\frac{[O_3]_{(ads_max)}K_{I1}}{1 + K_{I1}[O_3]_a}\right) \times (\rho \times [catalyst])\right)}{k_3[HCO_3^-] + k_{OH/TBA}[TBA]}\right)[O_3]$$
(Eq. 10)

$$[\bullet \text{OH}]_{ss} = \left(\frac{2k_1[OH^-] + \left((k_2) \times \left(\frac{[O_3]_{(adr-max)}K_I}{1 + K_{II}[O_3]_a}\right) \times (\rho \times [catalyst])\right)}{k_4[PO_4^{3-}] + k_{OH/TBA}[TBA]}\right)[O_3]$$
(Eq. 11)

As shown in Figure S6, the removal of ATZ decreased as the concentrations of HCO_3^-/CO_3^{2-} and PO_4^{3-} increased, which was completely inhibited at an initial concentration of 400 mg/L of $HCO_3^-/$ ${\rm CO_3}^{2}$ as ${\rm CaCO_3}$ and 100 mg/L of ${\rm PO_4}^{3-}$. The R_{ct} values determined at different initial HCO $_3$ ⁻/CO $_3$ ²⁻ (0 ~ 200 mg/L as CaCO $_3$) and PO $_4$ ³⁻ (0 ~ 15 mg/L) concentrations are shown in Figure S7A and S7C respectively. Further, k_3 and k_4 were determined from the slope of the plot $1/R_{ct}$ vs $[HCO_3^-/CO_3^{2-}]$ or $[PO_4^{3-}]$ (Figures S7B &S7D; Eqs S8 & S9, Text S4 (c)), which were found to be $8.31 \times 10^6 \,\mathrm{M}^{-1} \bullet \mathrm{s}^{-1}$ and $5.92 \times 10^5 \,\mathrm{M}^{-1} \bullet$ s⁻¹ respectively. The rate constant of HCO₃⁻/CO₃²⁻ with •OH determined in this study was close to the reported value (8.5 \times 10⁶ M⁻¹ \bullet s⁻¹) obtained in aqueous solutions (Yong and Lin, 2012). This indicates that the inhibitive effects on ATZ degradation exerted by HCO₃⁻/ CO₃²⁻ can mainly be ascribed to the homogeneous pathways, such as scavenging of •OH. On the other hand, the inhibition rate constant of PO₄³⁻ determined here is approximately 4–30 times as high as the reported values $(0.2\sim1.5\times10^5\,\mathrm{M}^{-1}\bullet\mathrm{s}^{-1})$ obtained in aqueous solutions (Buxton et al., 1988), implying that in addition to the •OH scavenging effects, interactions between phosphate anions and the catalysts, such as ligand exchange with the surface hydroxyl group of catalyst (Qi et al., 2013, 2008), may play an even more important role here. To this end, we further examined the density of surface adsorbed ozone (Text S5) in the presence of catalysts with and without $HCO_3^-/\ CO_3^{\ 2-}$ or $PO_4^{\ 3-}$. As shown in Fig. S8, while the steady-state density of surface adsorbed ozone remained relatively constant at different HCO3⁻/ CO3²⁻, the density of surface adsorbed ozone at steady-state decreased with the increase of PO₄³⁻ concentration, suggesting some adsorptive sites could have been taken up by PO₄³⁻ ions. Moreover, slower ozone decomposition was observed in the presence of $PO_4^{\,3-}$ compared with those in the presence of HCO_3^{-}/CO_3^{2-} or in the absence of both, which further supports the discussion above.

3.3.3. Determination of initiation (K_{I2}) and inhibition (K_{S2}) rate constants of NOM/EfOM

The composition, concentration, and chemistry of NOM/EfOM are highly variable and may differ from one water matrix to another. During ozonation processes, NOM/EfOM can affect the stability of O₃ by involving in both the direct reaction with O3 and the indirect oxidation with •OH and act as either initiators, promoters, or inhibitor (Jothinathan and Hu, 2018; Staehelin and Hoigne, 1985; Yong and Lin, 2013, 2012). For example, NOM/EfOM with some functional groups such as the electron-rich aromatic moieties and aliphatic unsaturated constituents could be easily oxidized by O₃ by electron transfer, accompanied by the formation of intermediate radical species (e.g. $O_3^{\bullet-}$) and subsequent generation of •OH, and thus play a role of initiator/promoter (Ji et al., 2015; Von Sonntag and Von Gunten, 2012; Wang et al., 2019; Yong and Lin. 2012). On the other hand, NOM/EfOM may act as the scavenger of radicals, resulting in inhibitory effects. Moreover, in heterogeneous processes, NOM/EfOM may be adsorbed on the catalyst surface and occupy/block the active sites (Ikhlag et al., 2015; Luo et al., 2015).

Because of the complex nature and consequently inevitable over-simplification when represented with one model compound (e.g. humic acid), here we quantitatively evaluate the effects of NOM/EfOM in real environmental matrices. In particular, since ROC used in this study was generated from SE (Section 2.2) and thus the bulk organics should share the same characteristics but at a higher concentration, experiments were conducted in SW and SE with the addition of ATZ and an external inhibitor of tert-butanol. Eq (6) becomes Eq (12) when NOM/EfOM acting as both initiators and inhibitors is considered:

$$[\bullet \text{OH}]_{ss} = \frac{2k_{1}[OH^{-}] + \left((k_{2}) \times \left(\frac{[O_{3}|_{cadsmax})K_{I1}}{1 + K_{I1}[O_{3}]_{a}}\right) \times (\rho \times [catalyst])\right) + k_{I2}[TOC]}{k_{.OH/TBA}[TBA] + k_{s2}[TOC] + k_{3}[HCO_{\overline{3}}] + k_{4}[PO_{4}^{3-}]} [O_{3}]$$
(Eq.12)

As all other parameters have been determined in previous sections, the rate constants associated with NOM/EfOM can be obtained by the reciprocal of Eq S10 (Text S4(d)) and from the slope and intercept of plots of $1/R_{ct}$ vs $k_{\bullet OH/TBA}$ [TBA] (Figure S9). It should be emphasized that K_{I2} and K_{S2} are dependent on the specific characteristics of NOM/EfOM, which may vary for different environmental matrices and should be used with caution. In addition, two-stage ozone decomposition kinetics, characterized by an initial high R_{ct} (~20 S) followed by a low R_{ct} stage, have been reported for ozonation of NOM-containing water (Buffle et al., 2006; Yong and Lin, 2016). Due to the limitation of the experimental setup here, we were unable to collect enough data during the rapid stage. Nonetheless, such two-stage kinetics was not obvious in our experiments (Figure S9) possibly because of the accelerating effect of catalysts/light irradiation on ozone decomposition.

Up till now, all the rate constants and parameters of Eq (6) have been determined and are summarized in Table 1. Therefore, the time-dependent profile of the target pollutant concentration during treatment can be estimated using Eq. (3) where the R_{ct} value can be calculated using Eq (S4).

3.4. Model validation

To validate the applicability and robustness of the kinetic model developed above, we monitored the degradation of another model compound, Atenolol (ATL), during plasmon-enhanced catalytic ozonation, in different water matrices and under different operating and solution chemical conditions. The experimental data was then compared with the model prediction. As shown in Fig. 4 (A-C), Fig. S10 (A, B) and Figure S11 (A, B), Eqs 3 & S4 successfully predict ATL removal in all three environmental matrices, as well as under different operating

Table 1 Calculated initiation rate constants of OH $^-$ (k_1), 0.5wt%Ag/MnFe₂O₄ catalysts (k_2 , K_{11}) NOM/EfOM (k_{12}), and inhibition rate constants of NOM/EfOM (k_{S2}), carbonate/bicarbonate (k_3), phosphate (k_4).

Environ. Matrices	Initiation rate constants $k_1(M^{-1}s^{-1}) \qquad \qquad k_2(M^{-1}s^{-1}) \qquad \qquad K_{\Pi}(M^{-1})$		$K_{11}(\mathrm{M}^{-1})$	$k_{12}(M^{-1}s^{-1})$	Inhibition rate conduction $k_{S2} (M^{-1}s^{-1})$	te constants $k_3 (\text{M}^{-1} \text{s}^{-1}) k_4 (\text{M}^{-1} \text{s}^{-1})$	
SW SE	144.6 6.4	$42 \times 10^8 \times I + 8.35 \times 10^{-3}$	1.37×10^5	0.314 0.089	$\begin{array}{c} 3.12 \times 10^6 \\ 0.86 \times 10^6 \end{array}$	8.31×10^6	5.92×10^5

Note: SW: surface water; SE: secondary effluent; I: photon flux (Einstein • L⁻¹ • s⁻¹); ρ: density of surface -OH groups (29.44 μmol/g for 0.5wt%Ag/MnFe₂O₄).

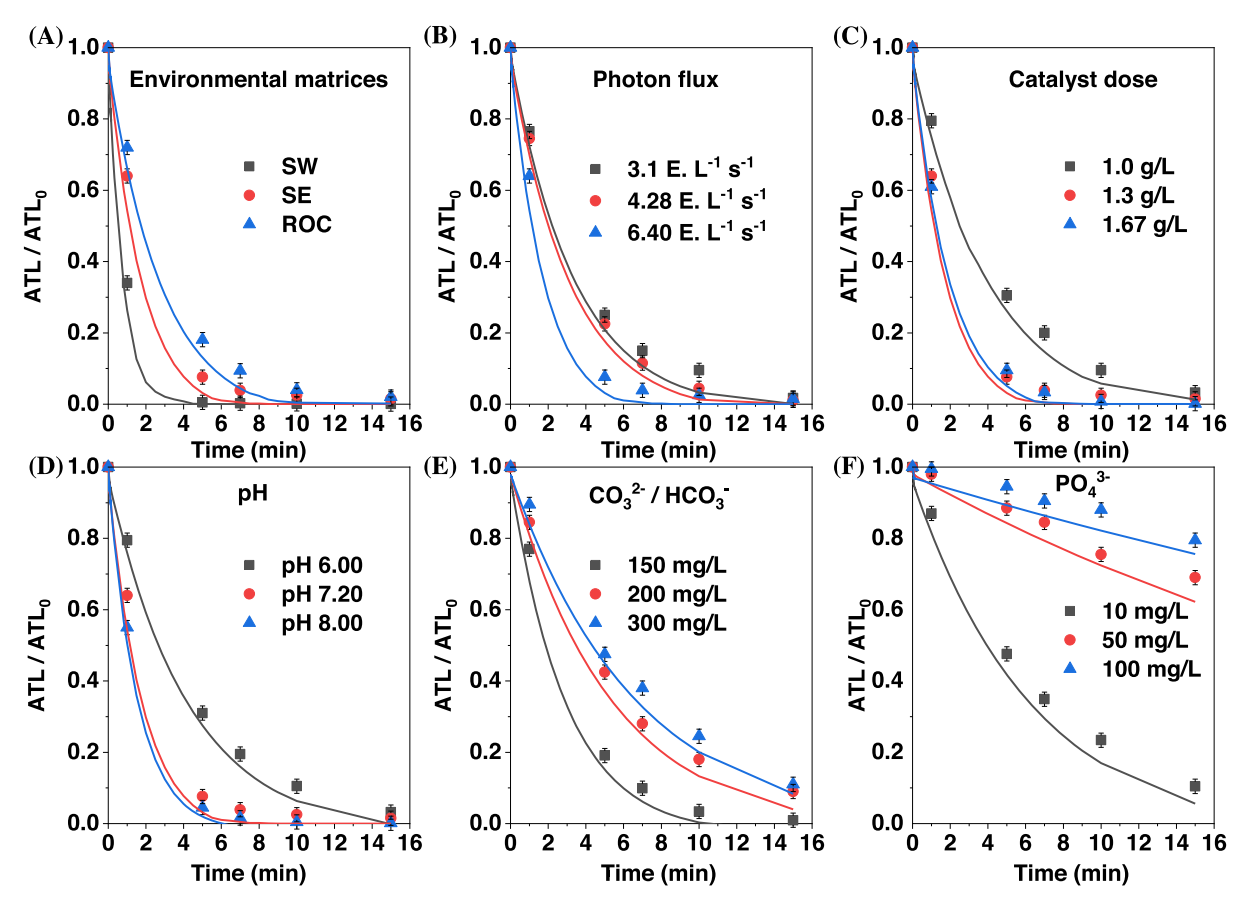


Fig. 4. Comparison of the experimental results (symbol) and the model predictions (solid line) for the removal of atenolol (ATL) in all three environmental matrices (A), under different operating conditions [photon flux (B) and catalyst dose (C)], and under different solution chemical conditions [pH (D), $\text{CO}_3^{2^-}/\text{HCO}_3^{-}$ (E), and PO₄^{3^-} (F)] during plasmon-enhanced catalytic ozonation [Experimental conditions: Initial ATL concentration: 2 mg/L; O₃/TOC_matrx (mass) = 0.85; working solution: 150 mL; photon flux (except B): 6.4×10^{-10} Einstein • L^{-1} • s^{-1} , catalyst dose (except C): 1.3 g/L; Results shown in B, C, D, E, F were obtained in SE].

conditions (i.e. photon flux and catalyst dose). We further examined ATL removal against model predictions under different solution chemical conditions signifying the most important influencing chemical species in environmental waters. As can be seen in Fig. 4(D-F), Figure S10(C-E) and Figure S11(C-E), a good agreement between the model prediction and experimental measurements was observed within the common concentration range of the selected species. The coefficients of determination (R^2) were summarized in Table S2 and a $R^2 > 0.95$ was obtained for all runs except those at high phosphate concentrations (50 and 100 mg/L) in SE and ROC, where the model tended to overestimate ATL removal. It is worth mentioning that phosphate has exhibited a significant inhibition effect at elevated concentrations. Therefore, although applications in SW or SE where phosphate is usually less than 20 mg/L should be no issue (Vu and Wu, 2020), pre-treatment for phosphate removal may be needed if the catalysts are used to treat matrices that contain high levels of phosphate.

While the model development and validation experiments discussed above were conducted at a relatively high ATL concentration (i.e. $2\,\text{mg/L}$) for the ease and accuracy of analytical analysis, we also examined the

treatment performance as well as the model prediction at an initial concentration of $10~\mu g/L$ with a low ozone dose. As shown in Fig. 5A, no ATL was detected (detection limit: $0.05~\mu g/L$) after $5~min~(O_3/TOC~(mass): 0.7)$, $10~min~(O_3/TOC~(mass): 1.0)$, and $15~min~(O_3/TOC~(mass): 1.1)$ treatment for SW, SE, and ROC respectively, demonstrating the high treatment efficiency of plasmon-enhanced catalytic ozonation processes in various environmental matrices under realistic conditions.

In addition to the potential high-energy consumption, formation of harmful byproducts is another concern of AOPs. In this study, we also monitored the formation of bromate (BrO $_3$ ⁻), a characteristic ozonation byproduct, during different treatment processes. It has been reported that less bromate was generated in the presence of solid catalysts (Zhang et al., 2011, 2008), and even less formation of bromate occurred in the plasmon-enhanced catalytic ozonation process in our previous tests conducted in tap water (Yang et al., 2021). Similar trends were observed in SW, SE, and ROC here, where 6.5, 10.2, and 12.1 μ g/L bromate was detected in SW, SE, and ROC after 15 min treatment with plasmon-enhanced catalytic ozonation (Fig. 6). Moreover, variations of concentrations of the main Br-containing species were recorded in

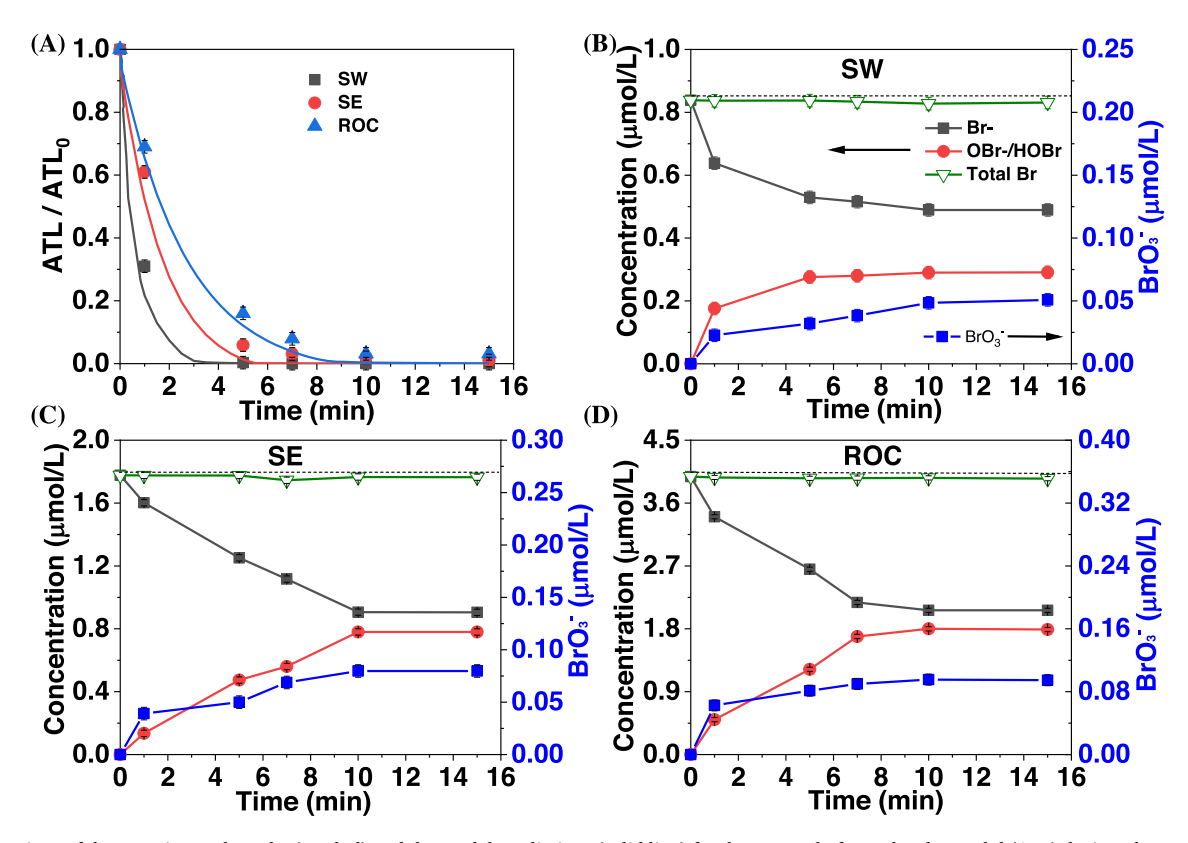


Fig. 5. Comparison of the experimental results (symbol) and the model predictions (solid line) for the removal of μ g/L level atenolol (ATL) during plasmon-enhanced catalytic ozonation (A); Concentration profiles of Br species and the corresponding bromine mass balance during plasmon-enhanced catalytic ozonation in SW (B), SE (C), and ROC (D) [Experimental conditions: Initial ATL concentration: 10μ g/L; O_3/TOC (mass) = 0.69 (SW, $5 \min$), 0.98 (SE, $10 \min$); 1.12 (ROC, $15 \min$), working solution: 150μ g/L; catalyst dose: 1.3μ g/L; light source: LEDs; photon flux 6.4×10^{-10} Einstein • 10μ g/L; 10μ

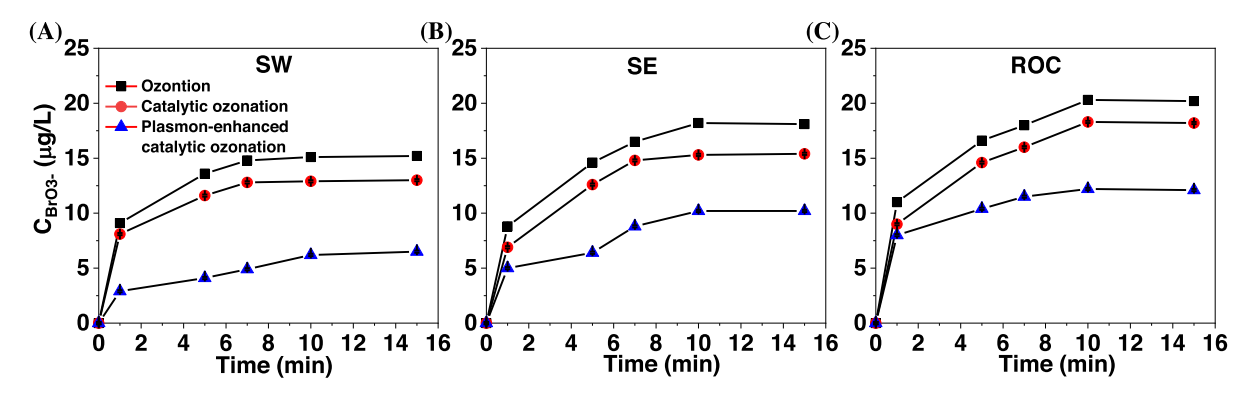


Fig. 6. Concentration profiles of BrO_3^- during ozonation, catalytic ozonation, and plasmon-enhanced catalytic ozonation in different environmental matrices: SW (A), SE (B), and ROC (C) [Experimental conditions: Initial ATL concentration: $10 \mu g/L$; O_3/TOC (mass) = 1.1; working solution: $150 \mu L$; catalyst dose: $1.3 \mu g/L$; light source: LEDs; photon flux (when irradiated): $6.4 \times 10^{-10} Einstein \cdot L^{-1} \cdot S^{-1}$].

different water matrices (Fig. 5(B–D)). Results suggest that three major bromine-containing species, i.e. Br-, HOBr/OBr-, and BrO_3^- , are present. Mass balance analysis on total Br content indicates minimum formation of bromated organic byproducts. While investigation of bromate formation and inhibition mechanism of this novel catalytic ozonation process is out of the scope of this study and is part of our ongoing research, it may be speculated that fast ozone decomposition and enhanced redox reactions on the catalyst surface are possibly responsible for the inhibition of bromate formation in the presence of catalysts and light irradiation. Nonetheless, the high removal efficiency and low byproduct formation demonstrates the great potential of plasmon-enhanced catalytic ozonation processes for water/wastewater treatment.

3.5. Estimation of energy consumption

Electrical energy per order (E_{EO} , kWh/m^3), defined as the electrical energy required to degrade the contaminant by one order magnitude in m^3 of treated water, is a commonly used figure-of-merit to characterize the energy consumption of AOPs (Bolton et al., 2001):

$$E_{EO} = \frac{P \times t \times 1000}{V \times \log\left(\frac{|C_0|}{|C_i|}\right)}$$
(Eq. 13)

Where P is the electrical energy input into the reactor, kW; t is the treatment time, h; V is the working solution volume, L; $[C]_0$ and $[C]_t$ are the initial concentration and the final concentration of the target

compound, respectively, mg/L.

When degradation of the target contaminant can be described with first-order kinetics with a reaction rate constant of k (Figure S12), Eq (13) can be written as:

$$E_{EO} = \frac{P \times 1000}{V \times 0.4343 \times k}$$
 (Eq. 14)

For the plasmon-enhanced catalytic ozonation process, both ozone generation (E_{EO-ozone}, kWh/m³) and light irradiation (E_{EO-LED}, kWh/m³) involve energy consumption. The electrical energy for ozone generation has been reported to be ~15 kWh/kg (Rosenfeldt et al., 2006; USEPA, 1999), which, together with ozone dose, can be used to calculate E_{EO-ozone}, E_{EO-LED} can be estimated based on the photon flux and the plug-efficiency of LEDs. Here we have estimated E_{EO} plasmon-enhanced catalytic ozonation processes under the treatment conditions of ATL shown in Fig. 5A, which is found to be 0.011 kwh/m³, 0.031 kwh/m³, and 0.086 kwh/m³ for SW, SE, and ROC, respectively (Text S6, Table S3). In addition, E_{EO} of different AOPs reported in the literature for the abatement of micropollutants in environmental matrices is also summarized in Table S3. While it is difficult to direct compare the results of different studies due to the huge difference in experimental setup and conditions, and characteristics of the model pollutants as well as the environmental matrices, it can be seen that the energy consumption of plasmon-enhanced catalytic ozonation was much lower than most of other AOPs.

4. Conclusion

This study evaluated the performance of a novel AOP, plasmonenhanced catalytic ozonation process, for the degradation of representative micropollutants in different environmental matrices including surface water (SW), secondary effluent (SE) and RO concentrate (ROC). A kinetic model combining the R_{ct} concept and expressions of steady state •OH concentrations has been successfully developed to describe and predict the time-dependent degradation profile of target pollutants under the influence of solution chemistry and operating conditions. Both bulk organic contents (NOM/EfOM) and some inorganic species commonly present in environmental waters (i.e. HCO₃⁻/CO₃²- ${\rm PO_4}^{3-}$) affected the treatment performance. In particular, while ${\rm HCO_3}^-/$ ${\rm CO_3}^{2-}$ mainly inhibits the target compound abatement via the homogeneous pathways such as scavenging of •OH, interactions between PO₄³⁻ and the catalysts, such as ligand exchange with the surface hydroxyl group of the catalyst which serve as the reactive sites for adsorptive ozone decomposition, play an important role in the inhibitive effects exerted by PO₄³⁻. Tests under environmentally relevant and realistic treatment conditions demonstrated high treatment efficiencies with low byproduct (e.g. bromate) formation (6.5–12.1 μg/L) and low energy consumption (E_{EO} 0.011–0.086 kWh/m³) for different matrices, underlining the great potential of plasmon-enhanced catalytic ozonation as an innovative AOP for advanced water/wastewater treatment.

Declaration of Competing Interest

The authors declare that they have no known competing financial interests or personal relationships that could have appeared to influence the work reported in this paper.

Acknowledgement

This work was financially supported by U.S. National Science Foundation (CBET-1606117). We also want to thank Hamilton Company for the Syringe Product Grant.

Supplementary materials

Supplementary material associated with this article can be found, in

the online version, at doi:10.1016/j.watres.2022.118072.

References

- Acero, J.L., Stemmler, K., Von Gunten, U., 2000. Degradation kinetics of atrazine and its degradation products with ozone and OH radicals: a predictive tool for drinking water treatment. Environ. Sci. Technol. 34, 591–597. https://doi.org/10.1021/ es990724e https://doi.org/.
- Bader, H., 1982. Determination of ozone in water by the indigo method: a submitted standard method. Ozone Sci. Eng. 4, 169–176. https://doi.org/10.1080/ 01919518208550955 https://doi.org/.
- Bergmann, M.E.H., Koparal, A.S., Iourtchouk, T., 2014. Electrochemical advanced oxidation processes, formation of halogenate and perhalogenate species: a critical review. Crit. Rev. Environ. Sci. Technol. 44, 348–390. https://doi.org/10.1080/ 10643389.2012.718948 https://doi.org/.
- Bolton, J.R., Bircher, K.G., Tumas, W., Tolman, C.a., 2001. Figures-of-merit for the technical development and application of advanced oxidation technologies for both electric- and solar-driven systems (IUPAC Technical Report). Pure Appl. Chem. 73, 627–637. https://doi.org/10.1351/pac200173040627 https://doi.org/.
- Buffle, M.-O., Schumacher, J., Salhi, E., Jekel, M., von Gunten, U., 2006. Measurement of the initial phase of ozone decomposition in water and wastewater by means of a continuous quench-flow system: Application to disinfection and pharmaceutical oxidation. Water Res 40, 1884–1894. https://doi.org/10.1016/j.watres.2006.02.026 https://doi.org/https://doi.org/.
- Buxton, G.V, Greenstock, C.L., Helman, W.P., Ross, A.B., 1988. Critical review of rate constants for reactions of hydrated electrons, hydrogen atoms and hydroxyl radicals (•OH/•O— in Aqueous Solution. J. Phys. Chem. Ref. Data 17, 513–886. https://doi.org/10.1063/1.555805 https://doi.org/
- Clesceri, E.W., rice, R.B.B., andrew, D.E.L.S., 2009. Standard methods for the examination of water and watewater. Am. public Heal. Assoc. Am. Water Work. Assoc. Water Environ. Fed. 22nd Editi.
- Elovitz, M.S., Von Gunten, U., 1999. Hydroxyl radical/ozone ratios during ozonation processes. I. The R(ct) concept. Ozone Sci. Eng. 21, 239–260. https://doi.org/ 10.1080/01919519908547239 https://doi.org/.
- Esplugas, S., Bila, D.M., Krause, L.G.T., Dezotti, M., 2007. Ozonation and advanced oxidation technologies to remove endocrine disrupting chemicals (EDCs) and pharmaceuticals and personal care products (PPCPs) in water effluents. J. Hazard. Mater. 149, 631–642. https://doi.org/10.1016/j.jhazmat.2007.07.073 https://doi.org/.
- Fatta-Kassinos, D., Vasquez, M.I., Kümmerer, K., 2011. Transformation products of pharmaceuticals in surface waters and wastewater formed during photolysis and advanced oxidation processes – Degradation, elucidation of byproducts and assessment of their biological potency. Chemosphere 85, 693–709. https://doi.org/ 10.1016/j.chemosphere.2011.06.082 https://doi.org/.
- Glaze, W.H., Kang, J., Douglas, H., 1987. The chemistry of water treatment processes involving ozone, hydrogen peroxide and ultraviolet radiation. Ozone Sci. Eng. 9, 335–352.
- Hodges, B.C., Cates, E.L., Kim, J.H., 2018. Challenges and prospects of advanced oxidation water treatment processes using catalytic nanomaterials. Nat. Nanotechnol. 13, 642–650. https://doi.org/10.1038/s41565-018-0216-x https://doi.org/.
- Ikhlaq, A., Brown, D.R., Kasprzyk-hordern, B., 2015. Applied catalysis B: environmental catalytic ozonation for the removal of organic contaminants in water on alumina. ". Applied Catal. B, Environ. 165, 408–418. https://doi.org/10.1016/j.apcatb.2014.10.010 https://doi.org/.
- Ji, Y., Dong, C., Kong, D., Lu, J., Zhou, Q., 2015. Heat-activated persulfate oxidation of atrazine: Implications for remediation of groundwater contaminated by herbicides. Chem. Eng. J. 263, 45–54. https://doi.org/10.1016/j.cej.2014.10.097 https://doi. org/
- Jiang, J.Q., Zhou, Z., Sharma, V.K., 2013. Occurrence, transportation, monitoring and treatment of emerging micro-pollutants in waste water - A review from global views. Microchem. J. 110, 292–300. https://doi.org/10.1016/j.microc.2013.04.014 https://doi.org/.
- Jothinathan, L., Hu, J., 2018. Kinetic evaluation of graphene oxide based heterogenous catalytic ozonation for the removal of ibuprofen. Water Res. 134, 63–73. https://doi. org/10.1016/j.watres.2018.01.033 https://doi.org/.
- Kasprzyk-Hordern, B., Ziółek, M., Nawrocki, J., 2003. Catalytic ozonation and methods of enhancing molecular ozone reactions in water treatment. Appl. Catal. B Environ. 46, 639–669. https://doi.org/10.1016/S0926-3373(03)00326-6 https://doi.org/.
- Luo, C., Ma, J., Jiang, J., Liu, Y., Song, Y., Yang, Y., Guan, Y., Wu, D., 2015. Simulation and comparative study on the oxidation kinetics of atrazine by UV/H2O2, UV/HSO5- and UV/S2O82. Water Res 80, 99–108. https://doi.org/10.1016/j.watres.2015.05.019 https://doi.org/.
- Márquez, G., Rodríguez, E.M., Beltrán, F.J., Álvarez, P.M., 2014. Solar photocatalytic ozonation of a mixture of pharmaceutical compounds in water. Chemosphere 113, 71–78. https://doi.org/10.1016/j.chemosphere.2014.03.093 https://doi.org/.
- Petrie, B., Barden, R., Kasprzyk-Hordern, B., 2014. A review on emerging contaminants in wastewaters and the environment: current knowledge, understudied areas and recommendations for future monitoring. Water Res 72, 3–27. https://doi.org/ 10.1016/j.watres.2014.08.053 https://doi.org/.
- Pinkernell, U., Von Gunten, U., 2001. Bromate minimization during ozonation: mechanistic considerations. Environ. Sci. Technol. 35, 2525–2531. https://doi.org/ 10.1021/es001502f https://doi.org/.
- Qi, F., Chen, Z., Xu, B., Shen, J., Ma, J., Joll, C., Heitz, A., 2008. Influence of surface texture and acid-base properties on ozone decomposition catalyzed by aluminum

- (hydroxyl) oxides. Appl. Catal. B Environ. 84, 684–690. https://doi.org/10.1016/j.apcatb.2008.05.027 https://doi.org/.
- Qi, F., Xu, B., Chen, Z., Feng, L., Zhang, L., Sun, D., 2013. Catalytic ozonation of 2-iso-propyl-3-methoxypyrazine in water by c -AlOOH and c -Al₂O₃: comparison of removal efficiency and mechanism. Chem. Eng. J. 219, 527–536. https://doi.org/10.1016/j.cej.2013.01.035 https://doi.org/.
- Rivera-Utrilla, J., Sánchez-Polo, M., Ferro-García, M.Á., Prados-Joya, G., Ocampo-Pérez, R., 2013. Pharmaceuticals as emerging contaminants and their removal from water. A review. Chemosphere 93, 1268–1287. https://doi.org/10.1016/j. chemosphere.2013.07.059 https://doi.org/.
- Rosenfeldt, E.J., Linden, K.G., Canonica, S., von Gunten, U., 2006. Comparison of the efficiency of {radical dot}OH radical formation during ozonation and the advanced oxidation processes O₃/H₂O₂ and UV/H₂O₂. Water Res 40, 3695–3704. https://doi.org/10.1016/j.watres.2006.09.008 https://doi.org/
- Staehelin, J., Hoigne, J., 1985. Decomposition of ozone in water in the presence of organic solutes acting as promoters and inhibitors of radical chain reactions. Environ. Sci. Technol. 19, 1206–1213. https://doi.org/10.1021/es00142a012 https://doi.org/.
- Staehelin, J., Holgné, J., 1982. Decomposition of ozone in water: rate of initiation by hydroxide ions and hydrogen peroxide. Environ. Sci. Technol. 16, 676–681. https://doi.org/10.1021/es00104a009 https://doi.org/.
- Sun, Q., Li, L., Yan, H., Hong, X., Hui, K.S., Pan, Z., 2014. Influence of the surface hydroxyl groups of MnO x /SBA-15 on heterogeneous catalytic ozonation of oxalic acid. Chem. Eng. J. 242, 348–356. https://doi.org/10.1016/j.cej.2013.12.097 https://doi.org/.
- USEPA, 1999. EPA Guidance Manual Alternative Disinfectants and Oxidants.
- Von Sonntag, C., Von Gunten, U., 2012. Chemistry of Ozone in Water and Wastewater Treatment from Basic Principles to Applications. IWA ppublishing, Londaon.
- Vu, C.T., Wu, T., 2020. Magnetic porous NiLa-layered double oxides (LDOs) with improved phosphate adsorption and antibacterial activity for treatment of secondary effluent. Water Res 175, 115679. https://doi.org/10.1016/j.watres.2020.115679 https://doi.org/.
- Wang, D., Xu, H., Ma, J., Giannakis, S., Lu, X., Chi, H., Song, S., Qi, J., 2019. Enhanced mineralization of atrazine by surface induced hydroxyl radicals over light-weight granular mixed-quartz sands with ozone. Water Res 149, 136–148. https://doi.org/ 10.1016/j.watres.2018.11.002 https://doi.org/.
- Wang, D., Xu, H., Ma, J., Lu, X., Qi, J., Song, S., 2018a. Strong promoted catalytic ozonation of atrazine at low temperature using tourmaline as catalyst: Influencing factors, reaction mechanisms and pathways. Chem. Eng. J. 354, 113–125. https://doi.org/10.1016/j.cej.2018.07.032 https://doi.org/.

- Wang, Z., Ma, H., Zhang, C., Feng, J., Pu, S., Ren, Y., Wang, Y., 2018b. Enhanced catalytic ozonation treatment of dibutyl phthalate enabled by porous magnetic Agdoped ferrospinel MnFe₂O₄ materials: Performance and mechanism. Chem. Eng. J. 354, 42–52. https://doi.org/10.1016/j.cej.2018.07.177 https://doi.org/.
- Wu, Y., Fang, Z., Shi, Y., Chen, H., Liu, Y., Wang, Y., Dong, W., 2019. Activation of peroxymonosulfate by BiOCl@Fe₃O₄ catalyst for the degradation of atenolol: Kinetics, parameters, products and mechanism. Chemosphere 216, 248–257. https://doi.org/10.1016/j.chemosphere.2018.10.012 https://doi.org/.
- Yang, W., Bunian, M., Chen, X., Heald, S., Yu, L., Wen, J., Lei, Y., Wu, T., 2021. Plasmon-enhanced catalytic ozonation for efficient removal of recalcitrant water pollutants. ACS ES&T Eng 1, 874–883. https://doi.org/10.1021/acsestengg.1c00020 https://doi.org/.
- Yang, W., Wu, T., 2019. Investigation of matrix effects in laboratory studies of catalytic ozonation processes. Ind. Eng. Chem. Res. 58, 3468–3477. https://doi.org/10.1021/ acs.iecr.8b05465 https://doi.org/.
- Yong, E.L., Lin, Y.P., 2016. Effects of pH value and temperature on the initiation, promotion, inhibition and direct reaction rate constants of natural organic matter in ozonation. RSC Adv 6, 18587–18595. https://doi.org/10.1039/c5ra19359a https://doi.org/.
- Yong, E.L., Lin, Y.P., 2013. Kinetics of natural organic matter as the initiator, promoter, and inhibitor, and their influences on the removal of ibuprofen in ozonation. Ozone Sci. Eng. 35, 472–481. https://doi.org/10.1080/01919512.2013.820641 https://doi.org/.
- Yong, E.L., Lin, Y.P., 2012. Incorporation of initiation, promotion and inhibition in the Rct concept and its application in determining the initiation and inhibition capacities of natural water in ozonation. Water Res 46, 1990–1998. https://doi.org/10.1016/j. watres.2012.01.025 https://doi.org/.
- Zhang, T., Chen, W., Ma, J., Qiang, Z., 2008. Minimizing bromate formation with cerium dioxide during ozonation of bromide-containing water. Water Res 42, 3651–3658. https://doi.org/10.1016/j.watres.2008.05.021 https://doi.org/.
- Zhang, T., Hou, P., Qiang, Z., Lu, X., Wang, Q., 2011. Reducing bromate formation with H+-form high silica zeolites during ozonation of bromide-containing water: Effectiveness and mechanisms. Chemosphere 82, 608–612. https://doi.org/10.1016/j.chemosphere.2010.10.078 https://doi.org/
- Zhao, H., Dong, Y., Wang, G., Jiang, P., Zhang, J., Wu, L., Li, K., 2013. Novel magnetically separable nanomaterials for heterogeneous catalytic ozonation of phenol pollutant: NiFe 2 O 4 and their performances. Chem. Eng. J. 219, 295–302. https://doi.org/10.1016/j.cej.2013.01.019 https://doi.org/.